Accepted Manuscript

Space charge and dielectric behavior of epoxy composite with sio_2-al_2o_3 nano-micro fillers at varied temperatures

Tian Fuqiang, Zhang Lin, Zhang Junliang, Peng Xiao

PII: S1359-8368(16)31098-8

DOI: 10.1016/j.compositesb.2017.01.062

Reference: JCOMB 4873

To appear in: *Composites Part B*

Received Date: 21 June 2016

Revised Date: 18 November 2016

Accepted Date: 28 January 2017

Please cite this article as: Fuqiang T, Lin Z, Junliang Z, Xiao P, Space charge and dielectric behavior of epoxy composite with sio_2-al_2o_3 nano-micro fillers at varied temperatures, *Composites Part B* (2017), doi: 10.1016/j.compositesb.2017.01.062.

Space Charge and Dielectric Behavior of Epoxy Composite with SiO_2-Al_2O_3 Nano-micro Fillers at Varied Temperatures

Tian Fuqiang, Zhang Lin, Zhang Junliang, Peng Xiao

School of Electrical Engineering, Beijing Jiaotong University, Beijing, 100044 China

ABSTRACT: Dielectric properties at high temperatures are important for epoxy resin used as insulation and package materials operating at varied temperatures in electrical apparatuses and electronic devices. We investigated the dielectric properties of epoxy resin and its composite with SiO_2-Al_2O_3 nano-micro fillers at varied temperatures by combined study of space charge distribution, complex dielectric permittivity and conduction current between 20 and 200 °C. The results show that space charge behavior in epoxy resin and its composite is dominated by electronic charge transport below the glass transition temperature T_g and by ion transport above T_g. The real and imaginary parts of complex permittivity increase to extremely high values at temperatures above T_g. The conduction current increases with a rise in temperature and shows an obvious transition from electronic charge transport below T_g to ionic charge transport above T_g. The composite shows weaker space charge accumulation, lower complex permittivity and conduction current than EP above T_g. Combined analysis of the results indicate that ion accumulation and transport dominate the dielectric properties of epoxy resin and its composite at high temperatures above T_g. The nano-micro fillers in the composite can significantly suppress the ions transport and accumulation.

KEYWORDS: epoxy resin, nano-micro fillers, space charge, dielectric behavior, varied temperatures

1. INTRODUCTION

Epoxy resin is widely used in various apparatuses from electronic devices to power machines. It is a kind of popular electrical insulating material for coils in motors and generators, cast-resin transformers, separators in gas-insulated switchgears and other machines[1-4]. It also shows extensive applications as base boards, adhesives, encapsulants, and packages for integrated circuit boards, power electronic modules, semiconductor devices, power lasers, light emitting diodes, solar cells and so on[5, 6]. However, with the continual increase of power density and miniaturization of electronic devices and power equipment, the power generated in devices or machines per unit volume has been increasing. For epoxy resin used for such purposes, heat dissipation and high temperature dielectric behavior have become the most critical problems that limit the performance and reliability of devices[7]. Then it is highly desirable to enhance thermal conductivity and high temperature dielectric properties of epoxy resin. High thermal conductivity can be readily achieved by incorporating large contents of various fillers with high thermal conductivity as reported by several studies[7-10]. It is found that the enhancement of thermal conductivity by using h-BN nanosheet is substantial at low filler loadings. At a loading of 5 wt%, the thermal enhancement factor is 113% for exfoliated h-BN nanosheets, and is only 28% for h-BN control[11]. High Al_2O_3 loadings up to 70 vol.% in the composites were achieved. The flexural strength and thermal conductivity of the Al_2O_3/epoxy composites were found to reach 305 MPa and 13.46 W/(m·K), respectively[12]. When the filler content was 25 vol%, the dielectric constant of composites was 51 which was eight times more than that of pure epoxy resin[13]. However, high temperature dielectric properties of epoxy resin and its composites are still not well understood yet.

At high temperatures and under high electric field, space charge accumulation will be intensified either due to electrode injection or impurity ionization, which can enhance the local electric field and exert a deteriorative effect on the dielectric properties of epoxy resin[14]. Space charge and dielectric behavior in epoxy resin and its composites at room and low temperatures have been intensively studied by many researchers[15-19]. However, few comprehensive studies at high temperature conditions have been reported, especially on temperature dependence of space charge evolution.

In this paper, space charge distributions, complex dielectric permittivity, and conduction currents were measured between 20 and 200 °C. Their correlations are investigated with focus on temperature depedence of charge transport and space charge accumulation.

2. EXPERIMENTAL

2.1 Materials

Materials used to make the samples are listed in Table 1. The base epoxy resin is diglycidyl ether of bisphenol-816B. Hardener 113 was used as a curing agent and its weight ratio to the epoxy resin is 30 to 100. The fillers include two kinds. One is Al_2O_3 in the shape of a sphere with a diameter of 0.4 μm which were added to a volume ratio of 30 vol%. The other is spherical SiO_2 particles with a diameter of 15 nm added to a ratio of 4 wt%. We use vol% for the microfiller since it is used to improve thermal conductivity, for which the volume ratio is important.

Firstly, the Al_2O_3 and SiO_2 fillers were mixed by a planetary centrifugal mixer (ARE-300, Thinky) for three minutes. Secondly, the filler mixture was added to epoxy resin and mixed using the same mixer for 10 minutes. After the mixture was degassed sufficiently in a vacuum oven at room temperature for about 30 minutes, it was mixed with the hardener for five minutes. It was then poured into a stainless steel mold and

pressed tightly. It was finally pre-cured at 70 °C for three hours and post-cured at 120 °C for antoher three hours. The sample obtained was naturally cooled down to room temperature. Hereafter, the neat epoxy resin is called EP and the composite is called EP30.

2.2 Scanning Electronic Microscope Imaging

Cross-section of the sample fractured in liquid nitrogen was observed by thermal field emission scanning electron microscope (JSM-7100F, JEOL) operated at 10 kV in order to observe the dispersion of microsized and nanosized fillers.

2.3 Complex Permittivity Measurement

Complex permittivity was measured by an impedance analyzer (126096, Solartron) at temperatures from 20 to 200 °C at intervals of 20 °C in a frequency range from 10^{-2} to 10^{6} Hz by applying an ac voltage of 3 V_{rms} to samples of 200 μm thick.

2.4 Conduction Current Measurement

The conduction current was measured sequentially by raising the temperature in a stepwise manner at intervals of 20 °C from 20 °C to 200 °C for 20 min at each temperature under the application of a dc electric field of 30 kV/mm. The current was measured by a digital electrometer (Advantest R8252). Both the measurements of complex permittivity and conduction current were carried out in a chamber filled with dry nitrogen gas at the atmospheric pressure to prevent the samples from oxidation at high temperatures. Furthermore, for these electrical measurements, aluminum electrodes with a diameter of 20 mm had been vacuum-evaporated on both sides of each sample. The thickness of the sample is 160 μm.

2.5 Space Charge Measurement

After the conduction current was measured at each temperature (20 - 200 °C) for 20 min (polarization process), the sample was cooled down to room temperature and the electric field was removed. Then space charge distribution was measured by a pulsed electroacoustic (PEA) device (Peanuts, Five Lab). Firstly, the measurement was conducted under a short-circuit condition. Secondly, it was repeated with a low electric field of 10 kV/mm with the same polarity as the electric field for the conduction current measurement. Thirdly, it was measured with the same electric field of the opposite polarity. The applications of these electric fields were done to determine the positions of electrodes and to distinguish space charges in the bulk from the charges on the electrodes.

In order to confirm the repeatability of the experimental results, at least two different samples are used for all the tests for each kind of the material.

3. RESULTS AND DISCUSSION

3.1 Nanoparticle Dispersion Characterization

Dispersion of the Al_2O_3 and SiO_2 nanoparticles in epoxy resin nano-micro composite is presented by SEM image in Figure 1. As showed by the SEM section image, the micro and nano particles are uniformly distributed in epoxy resin matrix. The particle size of Al_2O_3 is in the range 0.2 - 0.6 μm, with most particle size around 0.4 μm. The particle size of SiO_2 is in the range 10 - 30 nm and with most particle size around 15 nm.

3.2 Space Charge Distribution

Figure 2 shows space charge distributions in EP polarized at varied temperatures from 20 to 100 °C. At

20 °C, no observable bulk space charges accumulate considering the charge resolution of PEA device, which is about 1 C/m^3. At 40 °C, significant negative homocharges accumulate in front of the cathode as indicated by results under short-circuit or biased conditions with the same or opposite electric field direction to the polarizing electric field. The presence of space charge around the anode is not so clear at 40 °C if we examine only the short-circuited distribution. However, by applying the opposite electric field, it is clear that positive homocharges are present in front of the anode. Homocharges are usually ascribed to the electron and/or hole injection from the electrodes[20-22]. Therefore, it seems that both electrons and holes are injected at 40 °C. In addition, a small number of dispersed negative space charges can also be observed in the bulk near the anode. Homocharges around both cathode and anode electrodes have increased at 60 °C. At 80 and 100 °C, heterocharge accumulation around the cathode becomes significant besides electron and hole injection. Heterocharges are usually ascribed to transport and accumulation of mobile ions resulting from impurity ionization[23, 24]. The formation of heterocharges due to ionization can be further confirmed by dielectric permittivity and conduction current results later on.

Figure 3 shows space charge distributions in EP between 120 to 200 °C. Remarkably increasing positive charges accumulate around the cathode with an increase in polarization temperature. The maximum heterocharge density increases from about 5 C/m^3 at 100 °C to about 100 C/m^3 at 200 °C. Therefore, the accumulation of heterocharges due to ion transport and accumulation dominates the space charge behavior while homocharge formation due to electrode injection is obscured.

Figures 4 and 5 show space charge distributions in EP30 between 20 and 200 °C. The density of heterocharges is larger below 80 °C and smaller above 80 °C compared to that in EP. Furthermore, the increase of heterocharges above 100 °C is much less significant than that in EP. It seems that a small

number of homocharges due to injection are also present, but are generally obscured by heterocharges due to ionization especially at high temperatures from 120 to 200 °C. The concurrence of homocharges and heterocharges makes the space charge distributions and its dependence on temperature very complex and not as regular as that in EP.

3.3 Dielectric Behavior

Figures 6 and 7 show the complex relative permittivity spectra of EP and EP30 in a wide frequency range. As a significant feature, both ε_r' and ε_r'' increase rapidly with an increase in temperature above about 100 °C in both EP and EP30. For example, ε_r' is about 1900 and 1160 for EP and EP30, respectively.

There are several mechanisms that govern the frequency and temperature dependence of dielectric response in an insulating polymer. The dielectric response at frequencies below the GHz range mainly originates from the following three processes[25, 26] (i) microscopic rotational fluctuation of dipoles, (ii) translational diffusion of charge carriers, and (iii) separation and accumulation of charge carriers at interfaces between heterogeneous contacts. Polarization caused by charge hopping between two adjacent potentials is a typical process in the mechanism (ii). The mechanism (iii) is often called the Maxwell-Wagner (MW) polarization when it appears at an inner dielectric boundary layer on a mesoscopic scale, and called electrode polarization when it takes place at an interface between the sample and electrodes on a macroscopic scale. Considering the enormously high values of ε_r' and ε_r'', processes of (i) due to dipole polarization and (ii) due to ion translational diffusion should be ruled out. Since both epoxy resin and its composite shows large ε_r' and ε_r'' values, MW polarization at hterogeneous interface can also be excluded. As it has been found in electrolytes, electrode polarization due to ion blockage at the electrode-sample interface can yield extremely large ε_r' and ε_r'' values. This can also been supported by

corresponding space charge distributions, which shows that a large number of ions accumulated around the electrode at high temperatures. Therefore, it's reasonable to ascribe the increase in ε_r' to the accumulation of heteropolar ions in front of the electrodes. The increase in ε_r'' at high temepratures and low frequencies can be attributed to charge transport since it satisfies the relation $\varepsilon_r''=\sigma/2\pi f\varepsilon_0$ (σ is the electrical conductivity.) by showing a slope of -1 in the log ε_r'' - log f plot[25, 27]. At high temperatures and lower frequencies, since ions can have enough time to move to the electrode interface where they are blocked, so electrode polarization can increase ε_r' and ε_r'' to extremely high values due to induced numerous mirror charges on the electrode[28].

The phenomenon that the increasing in ε_r' and ε_r'' in EP and EP30 becomes significant with a rise in temperature can be explained as follows. It has been known that ions, more specifically sodium and chloride ions remaining from the synthesis procedure, i.e. the condensation of epichlorohydrin with bisphenol-A in the presence of alkali, are present in epoxy resin[29-33]. In addition, the unreacted hardener and nonreactive polar impurities in the hardener would be ionized at elevated temperatures[34-37] Although not shown here, thermal analysis shows that the glass transition temperature T_g is about 100 - 120 °C for the present epoxy resin[27, 38] It is well known that ionic conduction in polymers mainly takes place in amorphous regions, which can be enhanced by molecular movement. Since chain segment movement becomes active above T_g, so ion transport is assisted by local motions of polymer. Thus it is reasonable to deduce that ions can easily transport and accumulate around electrodes, forming the electrode polarization at temperatures above around T_g[25]. When the temperature is higher, more ions are activated, raising ε_r' more significantly. This is clearly confirmed in Figures 6 and 7 by the significant increase in ε_r' and ε_r'' with an increase in the temprature. Similar phenomena have also been observed in polymers containing mobile ions[39]. Therefore, electrode polarization and charge transport due to ions should be

responsible for the significantly large values of ε_r' and ε_r''.

At low temperatures below T_g, relaxation processes appearing clearly between 20 and 100 °C in both EP and EP30 as shown in Figures 6 and 7, which moves to higher frequency with the increase in temperature. Since ions are largely immobilized due to frozen chain segment motions below T_g, ions polarization can be excluded. In addition, considering the fact that the relaxation also occurs in pure epoxy resin, Maxwell-Wagner interfacial polarization due to charge accumulation at heterogeneous contacts can be ruled out. Theirfor, the relaxation process should be ascribed to the orientation of small polar groups such as those in side chains or side groups. The polar entities can be residual amines $–NH_2$ and –NH–, hydroxyl, epoxide rings, and other possible dipolar species[40, 41].

Figure 8 compares ε_r' and ε_r'' of EP and EP30 measured at 0.01 Hz and 1000 Hz between 20 and 200 °C. At 0.01 Hz, ε_r' shows a significant increase above 120 °C and above 100 °C in EP and in EP30 respectively, while ε_r'' shows a large increase between 100 and 120°C in EP and between 80 and 120°C in EP30. As discussed before, the increases in ε_r' and ε_r'' are attributed to the electrode polarization and charge transport enhanced by active chain section movement above T_g. The conclusion can be further supported by the temperature dependence of ε_r' and ε_r'' at 1000 Hz. A relaxation process related to the glass transition (often called α relaxation) can be clearly seen between 100 and 140 °C as a clear increase in ε_r' and a peak in ε_r'' around 120 °C. The relaxation is ascribed to local micro-Brownian motions of segments in the main chains[26]. With an increase in temperature, relaxation of the dipolar groups such as hydroxyl, ether, epoxides, chlorine, acid, and that of various groups like carboxyl, ester, amino, and others introduced by the hardener employed during the curing process are activated, resulting in an increase in ε_r' and ε_r'' at elevated temperatures[25]. If the temperature increases far above T_g, free volumes will be dramatically

increased[42-44]. This leads to the decrease in ε_r'' since polar groups in chain segments can move more freely and also leads to the decrease in ε_r' due to the decrease in the density[45-47]. These two phenomena can explain well the temperature profiles of ε_r' and ε_r'' shown in Figure 8. The validation of the glass transition process by temperature dependence of permittivity can also be found in other references[26, 48].

At 0.01 Hz, the composite EP30 shows smaller ε_r' at temperatures above 140 °C and smaller ε_r'' above 120 °C than EP. As mentioned above, the complex permittivity at high temperatures at low frequencies is dominated by the electrode polarization and charge transport. Therefore, the decrease in ε_r' and ε_r'' in the composites indicates that the transport of ions is suppressed by the addition of nanosized and microsized fillers. This is reasonable since molecular motions above T_g will be sterically hindered by the presence of fillers, which makes the ionic transport more difficult. On the other hand, it has been found that the addition of a large amount of nanosized and microsized fillers significantly increases the viscosity of the polymer, resulting in the formation of a considerable number of microvoids and hardener remains during the curing process[49]. The unreacted hardener will introduce impurity ionization while the microvoids are bound to enhance ion transport over a short range. Both of the two factors should account for the large complex permittivity values of EP30 at low temperatures.

3.4 Conduction Current

Figure 9 shows the conduction current behavior of EP and EP30 as a function of time measured at varied temperatures. The conduction current in both samples shows a significant increase at and above 100 °C. Figure 10 shows the reciprocal temperature dependence of conductivity calculated from steady state conduction current value, which was fitted to Arrhenius relation. The temperature dependence of conductivity also shows a significant transition around 100 °C. This indicates that the conduction current

should be controlled by different physical process. Considering the fact that space charge accumulation is dominated by electronic charges below 100 °C and ionic charges above 100 °C in EP as shown in Figures 2 and 3, we can deduce that the conduction current and conductivity is dominated by ions at high temperatures and by electronic charges at low temperatures. This further confirms that space charge, dielectric and conduction current behaviors at high temperatures are all governed by ion transport.

Generally, ions are transported in polymers via thermally activated hopping with a mobility that obeys the Arrhenius equation[50, 51]. EP30 shows lower activation energy (0.80 eV) than EP (1.06 eV) at high temperatures, implying that ion transport in EP is easier to be activated than in EP30. This is reasonable since chain movement above T_g is sterically hindered in EP30 due to nanosized and microsized fillers. EP shows higher activation energy at high temperature range than that at low temperature range since ion transport requires much higher energy to activate segmental motions of main chain compared to electronic charge transport.

4. CONCLUSIONS

Space charge and dielectric characteristics of epoxy resin and its composite with SiO_2-Al_2O_3 nano-micro fillers at varied temperatures were comprehensively studied via measurement of space charge, dielectric complex permittivity and conduction current between 20-200 °C. The following conclusions can be drawn.

(1)Space charge behavior in epoxy and epoxy composite with SiO_2-Al_2O_3 nano-micro fillers is dominated by electronic charge accumulation below glass transition temperature T_g and by ion accumulation above T_g;

(2)The enormous increase of real and imaginary parts of the complex permittivity above T_g is closely

related to electrode polarization as a result of ion accumulation around the electrode;

(3)The conduction current shows an obvious transition from electronic charge transport below T_g to ionic charge transport above T_g. The former shows much lower activation energy than the latter.

(4)The space charge distributions, complex permittivity, and conduction current are closely correlated and the all three processes are dominated by ion accumulation and transport above T_g.

(5)The epoxy composite shows weaker space charge accumulation, lower complex permittivity and conduction current than EP above T_g as a result of the steric hindrance effect of nano-micro fillers on epoxy chain segment movement and ion transport.

ACKNOWLEDGEMENT

This work is funded by Project 51507007 supported by National Natural Science Foundation of China. This work was completed in Waseda University in Japan with the help of Professor Ohki Yoshimichi.

REFERENCES

[1] Iyer G, Gorur R S, Richert R, et al. Dielectric properties of epoxy based nanocomposites for high voltage insulation[J]. IEEE Transactions on Dielectrics and Electrical Insulation. 2011, 18(3): 659-666.

[2] Krivda A, Tanaka T, Frechette M, et al. Characterization of epoxy microcomposite and nanocomposite materials for power engineering applications[J]. Electrical Insulation Magazine, IEEE. 2012, 28(2): 38-51.

[3] Halawani N, Auge J, Pruvost S, et al. Epoxy composites for insulating properties[C]. IEEE, 2015.

[4] Dakin T W. Application of epoxy resins in electrical apparatus[J]. IEEE Transactions on Electrical Insulation. 1974, EI-9(4): 121-128.

[5] Lu D, Wong C P. Materials for advanced packaging[M]. Springer, 2008.

[6] Johnston K, Pavuluri S K, Leonard M T, et al. Microwave and thermal curing of an epoxy resin for microelectronic applications[J]. Thermochimica Acta. 2015, 616: 100-109.

[7] Tanaka T, Kozako M, Okamoto K. Toward high thermal conductivity nano micro epoxy composites with sufficient endurance voltage[J]. Journal of International Council on Electrical Engineering. 2012, 2(1): 90-98.

[8] Gu J, Zhang Q, Dang J, et al. Thermal conductivity epoxy resin composites filled with boron nitride[J]. Polymers for Advanced Technologies. 2012, 23(6): 1025-1028.

[9] Hong J, Yoon S, Hwang T, et al. High thermal conductivity epoxy composites with bimodal distribution of aluminum nitride and boron nitride fillers[J]. Thermochimica Acta. 2012, 537: 70-75.

[10] Huang X, Jiang P, Tanaka T. A review of dielectric polymer composites with high thermal conductivity[J]. Electrical Insulation Magazine, IEEE. 2011, 27(4): 8-16.

[11] Lin Z, Mcnamara A, Liu Y, et al. Exfoliated hexagonal boron nitride-based polymer nanocomposite with enhanced thermal conductivity for electronic encapsulation[J]. Composites Science & Technology. 2014, 90(2): 123-128.

[12] Hu Y, Du G, Chen N. A novel approach for Al2O3/epoxy composites with high strength and thermal conductivity[J]. Composites Science & Technology. 2016, 124: 36-43.

[13] Luo B, Wang X, Zhao Q, et al. Synthesis, characterization and dielectric properties of surface functionalized ferroelectric ceramic/epoxy resin composites with high dielectric permittivity[J]. Composites Science & Technology. 2015, 112: 1-7.

[14] Montanari G C. Bringing an insulation to failure: the role of space charge [J]. IEEE Transactions on Dielectrics and Electrical Insulation. 2011, 18(2): 339-364.

[15] Das S, Gupta N. Charge trapping and transport phenomenon in aged and unaged epoxy resin and polyethylene[J]. International Transactions on Electrical Energy Systems. 2014.

[16] Das S, Gupta N. Effect of thermal and humidity ageing on space charge accumulation in epoxy resin[C]. IEEE, 2013.

[17] Castellon J, Nguyen H N, Agnel S, et al. Electrical properties analysis of micro and nano composite epoxy resin materials[J]. Dielectrics and Electrical Insulation, IEEE Transactions on. 2011, 18(3): 651-658.

[18] Wu C, Yan W, Phung B T. Influence of plasma-treated nanoparticles on space charge accumulation in epoxy resin insulation[C]. IEEE, 2013.

[19] Krivda A, Tanaka T, Frechette M, et al. Characterization of epoxy microcomposite and nanocomposite materials for power engineering applications[J]. Electrical Insulation Magazine, IEEE. 2012, 28(2): 38-51.

[20] Ieda M. Carrier Injection, Space Charge and Electrical Breakdown in Insulating Polymers[J]. IEEE Transactions on Electrical Insulation. 1987, EI-22(3): 261-267.

[21] Hori T, Kaneko K, Mizutani T, et al. Space charge distribution in low-density polyethylene with blocking layer[C]. Albuquerque, Nm: 2003.

[22] Neagu E R. Charge--Carrier injection and extraction at metal--Dielectric contact under an applied electric field[J]. Indian Journal of Pure & Applied Physics. 2008, 46(11): 809.

[23] Fuqiang T, Qingquan L, Xuan W, et al. Effect of Deep Trapping States on Space Charge Suppression in Polyethylene/ZnO Nanocomposite[J]. Applied Physics Letters. 2011, 99(14): 142903.

[24] Takada T, Hayase Y, Tanaka Y, et al. Space Charge Trapping in Electrical Potential Well Caused by Permanent and Induced Dipoles for LDPE/MgO Nanocomposite[J]. IEEE Transactions on Dielectrics and Electrical Insulation. 2008, 15(1): 152-160.

[25] Fuqiang T, Yoshimichi O. Charge transport and electrode polarization in epoxy resin at high temperatures[J]. Journal of Physics D: Applied Physics. 2014, 47(4): 45311.

[26] Kremer F, Schönhals A. Broadband dielectric spectroscopy[M]. Berlin: Springer-Verlag, 2003.

[27] Katayama J, Ohki Y, Fuse N, et al. Effects of nanofiller materials on the dielectric properties of epoxy nanocomposites[J]. IEEE Transactions on Dielectrics and Electrical Insulation. 2013, 20(1): 157-165.

[28] Sengwa R J, Sankhla S. Characterization of ionic conduction and electrode polarization relaxation processes in ethylene glycol oligomers[J]. Polymer Bulletin. 2008, 60(5): 689-700.

[29] Sheppard N F, Senturia S D. Dielectric properties of bisphenol-A epoxy resins[J]. Journal of Polymer Science Part B: Polymer Physics. 1989, 27(4): 753-762.

[30] Ulański J, Friedrich K, Boiteux G, et al. Evolution of ion mobility in cured epoxy‐amine system as determined by time‐of‐flight method[J]. Journal of applied polymer science. 1997, 65(6): 1143-1150.

[31] Friedrich K, Ulanski J, Boiteux G, et al. Time-of-flight ion mobility measurements in epoxy-amine systems during curing[J]. Dielectrics and Electrical Insulation, IEEE Transactions on. 2001, 8(3): 572-576.

[32] Makishima S, Nakano T, Koyama M, et al. Dielectric property of curing epoxy resin and application for casting processes[C]. IEEE, 1995.

[33] Lantz L, Pecht M G. Ion transport in encapsulants used in microcircuit packaging[J]. Components and Packaging Technologies, IEEE Transactions on. 2003, 26(1): 199-205.

[34] Cohen M, Kohn L S, Macdonald D I. Dielectric loss features of some epoxy resins[J]. Journal of Applied Polymer Science. 1963, 7(6): 2003-2023.

[35] Gonon P, Sylvestre A, Teysseyre J, et al. Dielectric properties of epoxy/silica composites used for microlectronic packaging, and their dependence on post-curing[J]. Journal of Materials Science: Materials in Electronics. 2001, 12(2): 81-86.

[36] Tomer V, Polizos G, Manias E, et al. Epoxy-based nanocomposites for electrical energy storage. I: Effects of montmorillonite and barium titanate nanofillers[J]. Journal of Applied Physics. 2010, 108(7): 74116.

[37] Polizos G, Tomer V, Manias E, et al. Epoxy-based nanocomposites for electrical energy storage. II: Nanocomposites with nanofillers of reactive montmorillonite covalently-bonded with barium titanate[J]. Journal of Applied Physics. 2010, 108(7): 74117.

[38] Thelakkadan A S, Coletti G, Guastavino F, et al. Thermomechanical and Electrical Characterization of Epoxy-Organoclay Nanocomposites[J]. Polymer Engineering and Science. 2012, 52(5): 1037-1046.

[39] Fuse N, Sato H, Ohki Y, et al. Effects of Nanofiller Loading on the Molecular Motion and Carrier Transport in Polyamide[J]. IEEE Transactions on Dielectrics and Electrical Insulation. 2009, 16(2): 524-530.

[40] Baziard Y, Breton S, Toutain S, et al. Dielectric properties of aluminium powder-epoxy resin composites[J]. European polymer journal. 1988, 24(6): 521-526.

[41] Deng Y, Martin G C. Analysis of the cure‐dependent dielectric relaxation behavior of an epoxy resin[J]. Journal of Polymer Science Part B: Polymer Physics. 1994, 32(12): 2115-2125.

[42] Turnbull D, Cohen M H. Free volume model of the amorphous phase: glass transition[J]. The journal of chemical physics. 1961, 34(120): 120-125.

[43] Cohen M H, Grest G S. Liquid-glass transition, a free-volume approach[J]. Physical review B. 1979, 20(3): 1077-1098.

[44] Turnbull D, Cohen M H. On the Free-Volume Model of the Liquid-Glass Transition[J]. The journal of chemical physics. 1970, 52(6): 3038-3041.

[45] Ramajo L, Reboredo M, Castro M. Dielectric response and relaxation phenomena in composites of epoxy resin with BaTiO3 particles[J]. Composites Part A: Applied Science and Manufacturing. 2005, 36(9): 1267-1274.

[46] Roy M, Nelson J K, Maccrone R K, et al. Polymer nanocomposite dielectrics-The role of the interface[J]. IEEE Transactions on Dielectrics and Electrical Insulation. 2005, 12(4): 629-643.

[47] Tsangaris G M, Psarras G C, Kontopoulos A J. Dielectric permittivity and loss of an aluminum-filled epoxy resin[J]. Journal of non-crystalline solids. 1991, 131(133): 1164-1168.

[48] Neagu E, Pissis P, Apekis L, et al. Dielectric relaxation spectroscopy of polyethylene terephthalate (PET) films[J]. Journal of Physics D: Applied Physics. 1999, 30(11): 1551-1560.

[49] Wang Z, Iizuka T, Kozako M, et al. Development of epoxy/BN composites with high thermal conductivity and sufficient dielectric breakdown strength partI-sample preparations and thermal conductivity[J]. IEEE Transactions on Dielectrics and Electrical Insulation. 2011, 18(6): 1963-1972.

[50] Abdel-Wahab F. Unified hopping model for dc and ac conduction in chalcogenide glasses[J]. Philosophical Magazine B. 2002, 82(12): 1327-1333.

[51] Egginger M, Schwödiauer R. Analysis of mobile ionic impurities in polyvinylalcohol thin films by thermal discharge current and dielectric impedance spectroscopy[J]. AIP Advances. 2012, 2(4): 42152.

Table 1 Materials used for sample preparation

Material	Provider	Average filler size
Epoxy 816B	Mitsubishi Chemical, Japan	–
Hardener 113	Mitsubishi Chemical, Japan	–
Al_2O_3 (cubic)	Admatechs, Japan	0.4 μm
SiO_2	Aerosil, Japan	15 nm

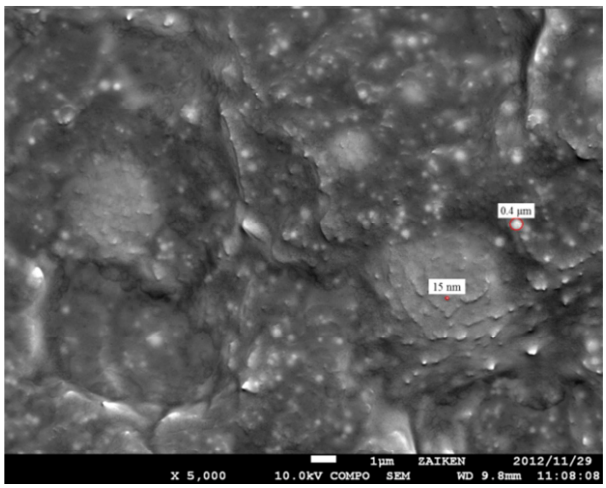

Figure 1 Sectional morphology graph of epoxy resin nano-micro composite.

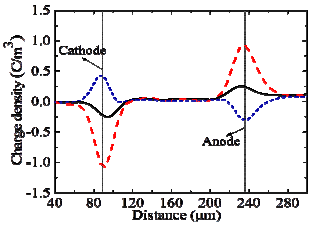

(a) polarized at 20 °C

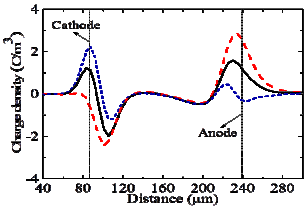

(b) polarized at 40 °C

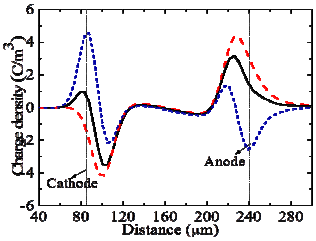

(c) polarized at 60 °C

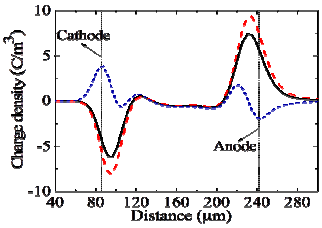

(d) polarized at 80 °C

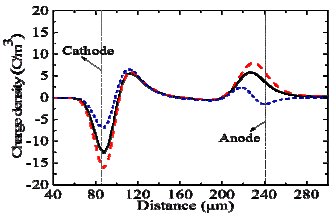

(e) polarized at 100 °C

Figure 2 Space charge distribution in EP polarized at temperatures between 20 and 100 °C. The curves represent the distributions observed when the sample was short-circuited (—), or biased in the direction same as (---) or opposite to (⋯) the polarizing electric field.

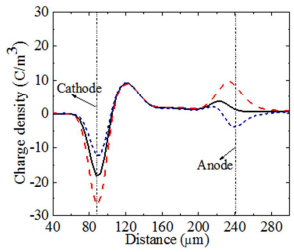

(a) polarized at 120 °C

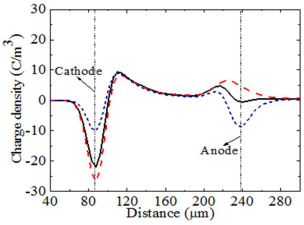

(b) polarized at 140 °C

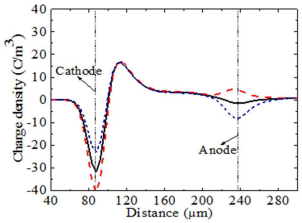

(c) polarized at 160 °C

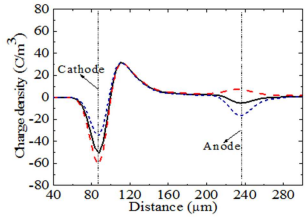

(d) polarized at 180 °C

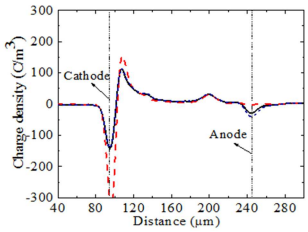

(e) polarized at 200 °C

Figure 3 Space charge distribution in EP polarized at temperatures between 120 and 200 °C. The curves represent the distributions observed when the sample was short-circuited (—), or biased in the direction same as (---) or opposite to (⋯) the polarizing electric field.

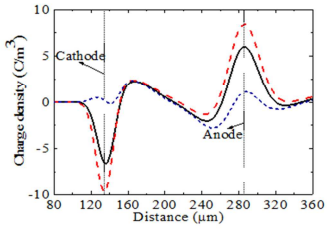

(a) polarized at 20 °C

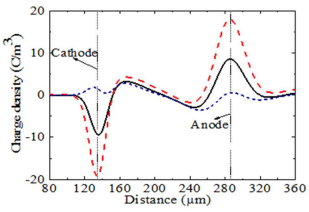

(b) polarized at 40 °C

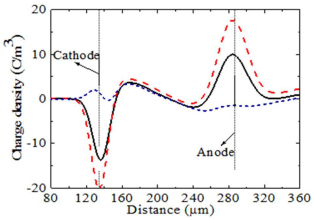

(c) polarized at 60 °C

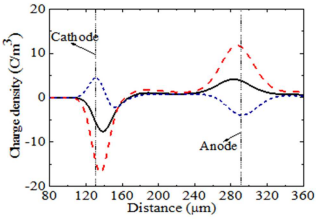

(d) polarized at 80 °C

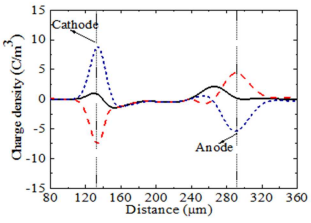

(e) polarized at 100 °C

Figure 4 Space charge distribution in EP30 polarized at temperatures between 20 and 100 °C. The curves represent the distributions observed when the sample was short-circuited (—), or biased in the direction same as (---) or opposite to (⋯) the polarizing electric field.

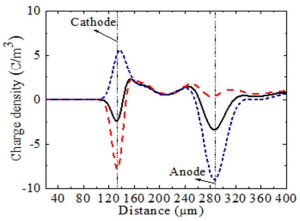

(a) polarized at 120 °C

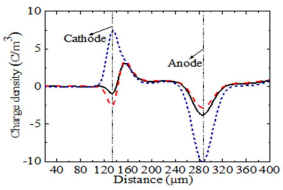

(b) polarized at 140 °C

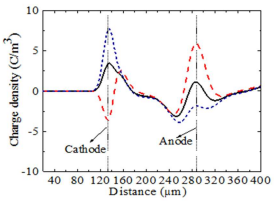

(c) polarized at 160 °C

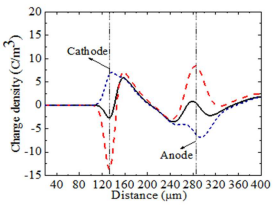

(d) polarized at 180 °C

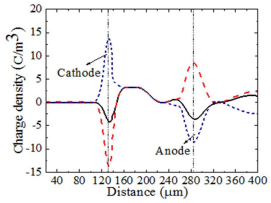

(e) polarized at 200 °C

Figure 5 Space charge distribution in EP30 polarized at temperatures between 120 and 200 °C. The curves represent the distributions observed when the sample was short-circuited (—), or biased in the direction same as (---) or opposite to (⋯) the polarizing electric field.

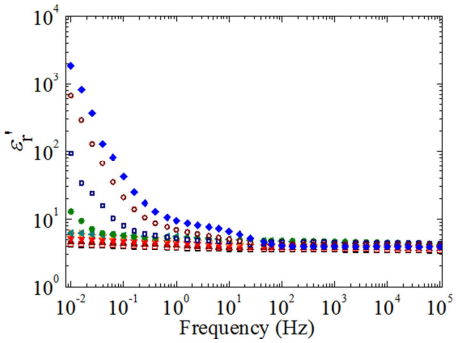

(a)

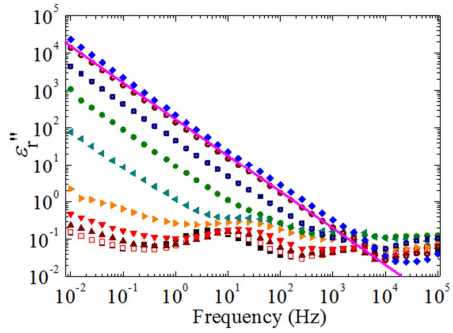

(b)

Figure 6 Real part () and imaginary part () of the complex permittivity of epoxy resin, each as a function of frequency, measured at different temperatures. The symbols represent 20 (■), 40 (□), 60 (▲), 80 (▼), 100 (►), 120 (◄), 140 (●), 160 (◘), 180 (o), and 200 (♦).

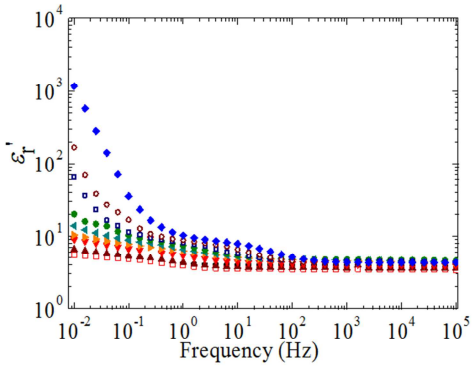

(a)

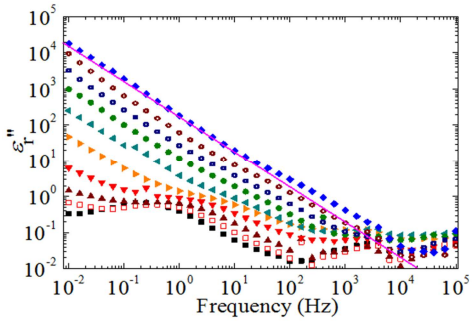

(b)

Figure 7 Real part () and imaginary part () of the complex permittivity of EP30, each as a function of frequency, measured at different temperatures. The symbols represent 20 (■), 40 (□), 60 (▲), 80 (▼), 100 (►), 120 (◄), 140 (●), 160 (◘), 180 (o), and 200 (♦).

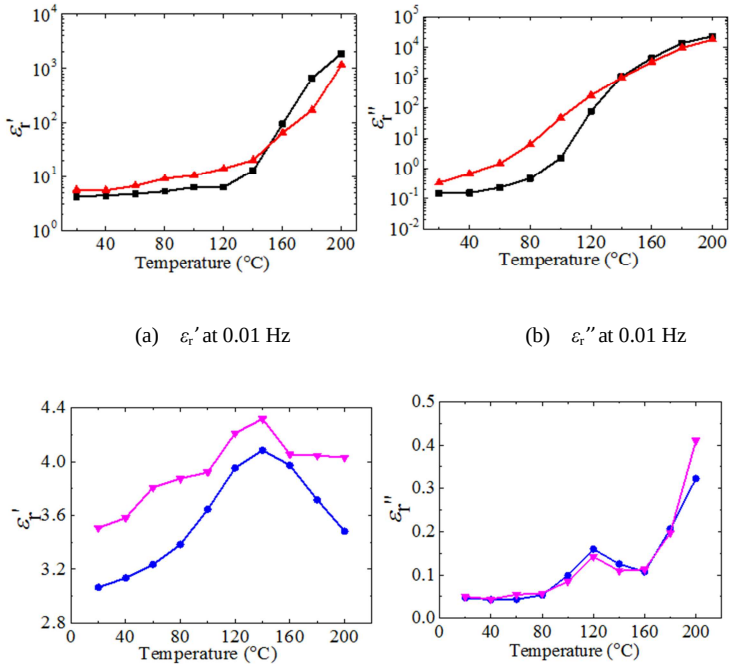

(a) ε_r' at 0.01 Hz (b) ε_r'' at 0.01 Hz

(c) ε_r' at 1000 Hz (d) ε_r'' at 1000 Hz

Figure 8 Real part (a, ε_r') and imaginary part (b, ε_r'') of the complex permittivity, each as a function of temperature, at two typical frequencies. The symbols represent EP at 0.01 Hz (■), EP at 1000 Hz (●), EP30 at 0.01 Hz (▲), and EP30 at 1000Hz (▼).

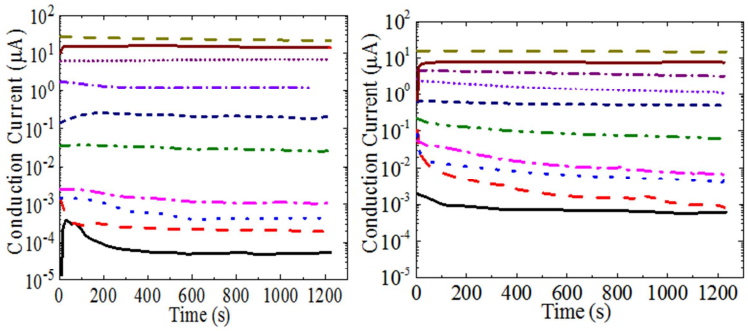

(a) (b)

Figure 9 Conduction current of EP (a) and EP30 (b) as a function of time. The lines represent 20 (——), 40 (- - - - -), 60 (· · ·), 80 (- · -), 100 (- · · · -), 120 (——), 140 (- - -), 160 (), 180 (——), and 200 (- - - -).

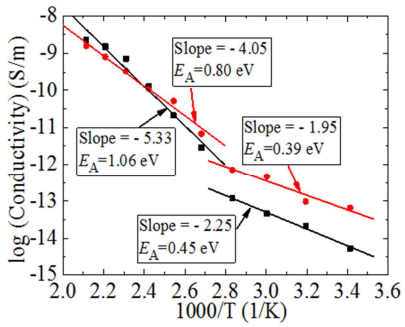

Figure 10 Arrhenius fitting of the conductivity calculated from the conduction current. E_A: activation energy. The symbols represent EP (■), EPN (●). Solid lines are the fitted curves.